STRUCTURES AND MATERIALS FOR FINITE LIFETIME

By N. J. Hoff

Division of Aeronautical Engineering
Stanford University, Stanford, California

Summary—The aerodynamic heating accompanying supersonic and hypersonic flight renders design for infinite lifetime impossible. At moderately high temperatures creep sets in and causes rupture in tension and buckling in compression, even under relatively small loads if they act for a sufficiently long time. At extremely high temperatures the structural material, or its protective covering, melts, vaporizes, sublimes, or burns. The analyst must be able to calculate the lifetime of the structural elements in order to ensure the safety of the structure. A few simple methods of analysis are presented in the report with the aid of which approximate calculations of the lifetime can be carried out.

NOTATION

a	constant; non-dimensional deflection amplitude; thermal diffusivity
b	thickness of wall
A	area
B	constant in Ramberg–Osgood relationship
c	specific heat
$\bar{c}_p$	average specific heat at constant pressure of gas mixture
C	constant; aerodynamic coefficient
D_{12}	coefficient of mass diffusion of species 1 into species 2
E	modulus
f	function
g	function
h	depth of idealized column section; external heat transfer coefficient
H	heating rate
I	integral; moment of inertia
k	constant
K	constant; thermal conductivity
L	length of bar or column; latent heat of melting
Le	Lewis–Semenov number defined in equation (114)

The work here presented was supported in whole by the United States Navy under Contract No. Onr 225(30) monitored by the Mechanics Branch of the Office of Naval Research.

m exponent of time in creep law; Landau's parameter defined in equation (107); mass transfer rate
M bending moment
n exponent of stress in creep law; integer
p integer; exponent in Ramberg–Osgood relationship; pressure
P load
$R = 1 + \epsilon$
s constant in exponential creep law; distance of ablating surface from origin of co-ordinates
t time
T temperature
u velocity component in x-direction
v velocity component in y-direction
V velocity of ablation
W weight
x variable; co-ordinate
y variable; co-ordinate
β constant in Andrade's law
δ thickness of layer of molten material
Δ increment
ϵ strain; emissivity
κ curvature; constant in Andrade's law
λ constant in creep law
μ coefficient of viscosity
ρ radius of gyration of section; density
σ stress; Boltzmann's radiation constant
τ shear stress
Φ heat flux

The following symbols, when used as subscripts, indicate or refer to:

cr critical
D drag
eff effective
E Euler
i interface
m melting
n natural
t tangent
u ultimate
0 initial or nominal value
00 initial value before elastic deformations
1 concave flange
2 convex flange

1. INTRODUCTION

BEFORE World War II the duty of the designer was to provide the airplane with a structure which would not fail under the loads expected in flight or at landing. Only comparatively recently was he given permission to hedge by stipulating a maximum number of hours of flying for which his guarantee would be valid; this change occurred when very thin-walled metal structures and ultra-high-strength aluminum alloys combined to bring about fatal failures due to fatigue.

The trend away from the concept of safety *ad infinitum* is now accelerating because the high temperatures accompanying supersonic and hypersonic flight make it impossible to build structures for anything but a finite lifetime. At the same time most missiles are required to make only a single flight and that even of rather short duration. To provide such a missile with a structure that would outlive the mission by a large factor, would be obviously a waste of weight, and thus also of fuel and money.

The purpose of this report is to discuss some of the factors that have recently attained importance in restricting the lifetime of airplane, missile, and spacecraft structures. No further mention will be made of fatigue as that topic has been amply treated in the literature of "cold" structures.

The first effect typical of "hot" structures that affects lifetime is the phenomenon of creep. It is well known that a metal test specimen subjected to a constant tensile load continues to increase in length with time if the temperature is high enough. Eventually the specimen fractures without any increase in load. The time at which fracture takes place, the critical time, is obviously of concern to the structural designer. The situation is similar with a column subjected to a compressive load which may be perfectly capable of supporting the load when it is applied but nevertheless it will buckle after a certain length of time, again referred to as the critical time.

These phenomena, described here and first explored in connection with bars, occur also with beams, frames, plates and shells. All these structural elements fracture, bulge, and collapse in the presence of creep when the loads are acting on them for a sufficiently long time.

The rate of attrition becomes even larger in bodies re-entering the atmosphere from outer space. Witness to the destructive power of the high-heating rates thus encountered are the meteors which melt, burn and evaporate in the air. The airplane designer must learn how to control these phenomena if he is to succeed in bringing back to the surface of the earth vehicles, and eventually vehicles containing human beings.

2. CREEP RUPTURE OF TENSILE BARS

A. Basic Concepts and Theoretical Derivation

Probably the most obvious limit of the useful life of a structural element operating at a high temperature is the time at which a bar, subjected to

tension, fractures in consequence of creep. The phenomenon was observed in 1910 by Andrade[1] who also gave a physical explanation of tertiary creep and fracture. He pointed out that the elongation of the bar from its original length L_0 to a length L at time t must be accompanied by a decrease in the cross-sectional area as creep takes place without a substantial change in volume. If the engineering strain is ϵ at time t, the length L is

$$L = L_0(1 + \epsilon) \tag{1}$$

and the new cross-sectional area A must be

$$A = A_0/(1 + \epsilon) \tag{2}$$

if A_0 was the original cross-sectional area. It follows from equations (1) and (2) that the volume remains constant in this process:

$$LA = L_0A_0 \tag{3}$$

But a decrease in the value of the cross-sectional area results in an increase in the tensile stress if the load P is constant. At the beginning of the test the stress is

$$\sigma_0 = P/A_0 \tag{4}$$

while at t

$$\sigma = P/A = \sigma_0(1 + \epsilon) \tag{5}$$

The increase in stress causes an increase in the strain rate which becomes noticeable when the engineering strain ϵ is a few per cent. The increasing strain rate indicates the beginning of the third phase of the creep process which generally leads to failure after a comparatively short time, namely as soon as the increasing stress in the decreasing cross-section reaches the value of the ultimate stress of the material at the test temperature.

Andrade proved his conjecture by employing a shaped weight partially submerged in water. The shape was devised in such a manner that the increase in buoyancy with increasing elongation exactly compensated for the decrease in cross-sectional area, and thus the stress remained constant during the entire test. In consequence the strain rate did not change and the secondary phase of creep extended up to fracture.

Andrade published an empirical formula derived from his experiments:

$$L = L_0(1 + \beta t^{1/3})e^{\kappa t} \tag{6}$$

where L is the length of the bar at time t, L_0 the same quantity at the beginning of the test ($t = 0$), t is time, and β and κ are constants for a constant stress and a constant temperature. When t is large, this relationship reduces to

$$(1/L)\,(\mathrm{d}L/\mathrm{d}t) = \epsilon_n = \kappa = \text{constant} \tag{7}$$

which can easily be stated in the words that the time rate of change of the natural strain is constant. When the strain does not exceed a few per cent, this is equivalent to the generally accepted secondary creep law according to which the time rate of change of the (engineering) strain is constant (provided the stress and the temperature remain constant).

In most practical applications the load acting on the element is constant

rather than the stress. In such a case the calculation of the time necessary for rupture to take place is not difficult; the fundamental considerations needed for it were presented by the author in Ref. 2. The secondary creep law can be given in the form

$$d\epsilon/dt = \dot{\epsilon} = f(\sigma) \tag{8}$$

where $f(\sigma)$ indicates an empirical function of the stress at a constant temperature. But in the constant load test the stress increases with time as ϵ in equation (5) increases with time. Hence σ must be replaced by $\sigma_0(1 + \epsilon)$ in equation (8). Similarly, the large deformations preceding rupture necessitate the substitution of the natural strain

$$\epsilon_n = \log (1 + \epsilon) \tag{9}$$

where log is the natural logarithm, in place of the engineering strain ϵ. Thus equation (8) becomes

$$(d/dt)[\log (1 + \epsilon)] = f[\sigma_0(1 + \epsilon)] \tag{10}$$

The justification of this creep law lies in its logic as well as in its agreement with Andrade's observations [1, 3].

From equation (10) a simple graphical procedure can be developed for the determination of the critical time under a constant load. If, for the sake of simplicity, the notation

$$R = (1 + \epsilon) \tag{11}$$

is introduced, in the differential equation

$$(d/dt)(\log R) = f(\sigma_0 R) \tag{12}$$

the variables can be separated:

$$dt = \frac{d(\log R)}{f(\sigma_0 R)} \tag{13}$$

At the beginning of the test $\epsilon = 0$ and thus $R = 1$; at the end of the test

$$R_{cr} = 1 + \epsilon_{cr} = \sigma_u/\sigma_0 \tag{14}$$

Hence the critical time is

$$t_{cr} = \int_1^{\sigma_u/\sigma_0} \frac{d(\log R)}{f(\sigma_0 R)} \tag{15}$$

Because of the non-linearity of the creep law the deformations begin slowly, but they proceed very rapidly as soon as they become noticeable. For this reason equation (15) can often be replaced by

$$t_{cr} \simeq \int_1^{\infty} \frac{d(\log R)}{f(\sigma_0 R)} \tag{16}$$

without a significant loss in accuracy. Since

$$d(\log \sigma) = d\sigma/\sigma = d(\sigma_0 R)/\sigma_0 R = d(\log R) \tag{17}$$

equation (16) can be written in the form

$$t_{cr} \simeq \int_{\sigma_0}^{\infty} \frac{d(\log \sigma)}{f(\sigma)} = \int_{\sigma_0}^{\infty} \frac{d(\log \sigma)}{\dot{\epsilon}} \tag{18}$$

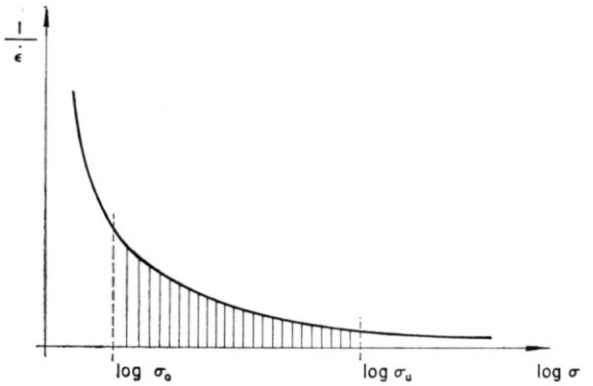

FIG. 1. Graphic determination of creep rupture time.

In Fig. 1 the reciprocal of the experimental steady creep rate is plotted against the logarithm of the stress at which it was measured. The area under this curve, taken between the ordinates log σ_0 and log σ_u where σ_u is the ultimate stress of the material at the test temperature, is the critical time. Often it does not differ significantly from the area under the curve between log σ_0 and infinity.

B. Comparison with Experiment

In Figs. 2 to 5 the results of graphic-numerical integrations are compared with experiment. The solid lines represent the experimental information on steady creep rate and creep rupture time while the dashed line is the critical time calculated by a numerical-graphic integration in accordance with equation (18). Theory and experiment are in satisfactory agreement in the case of pure aluminum (Figs. 2 and 3) but the difference between them is significant in the case of 75S-T6 aluminum alloy (Figs. 4 and 5).

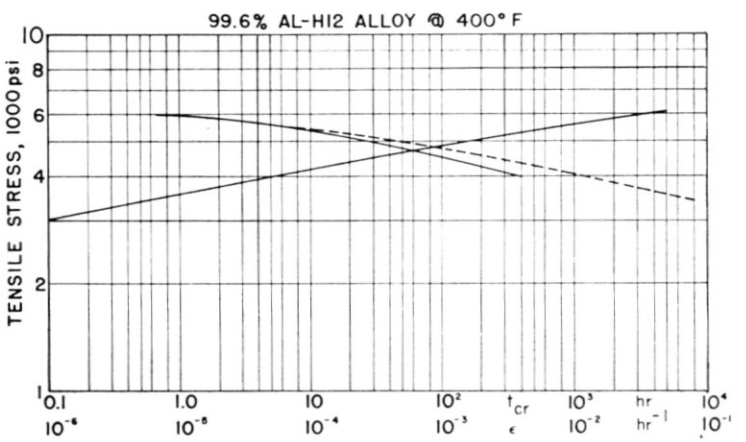

FIG. 2. Steady creep rate and rupture time.

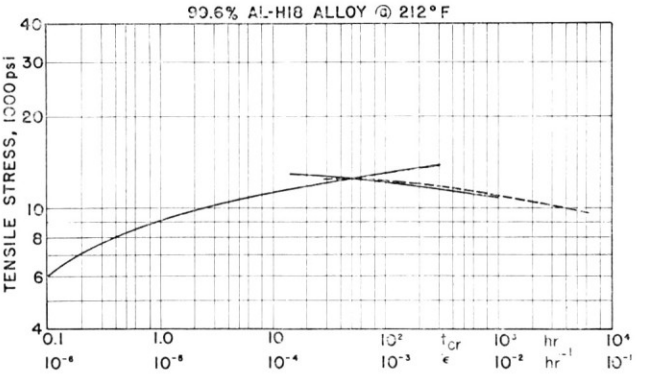

FIG. 3. Steady creep rate and rupture time.

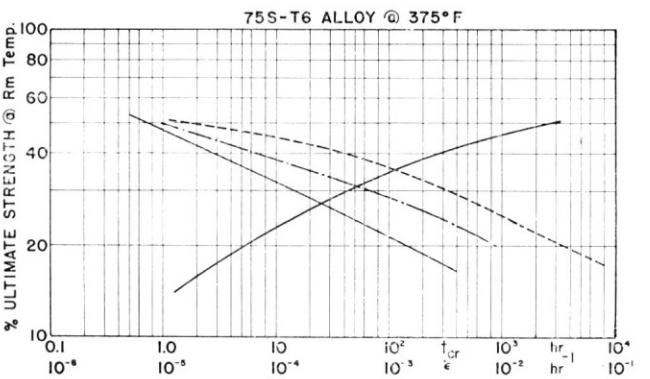

FIG. 4. Steady creep rate and rupture time.

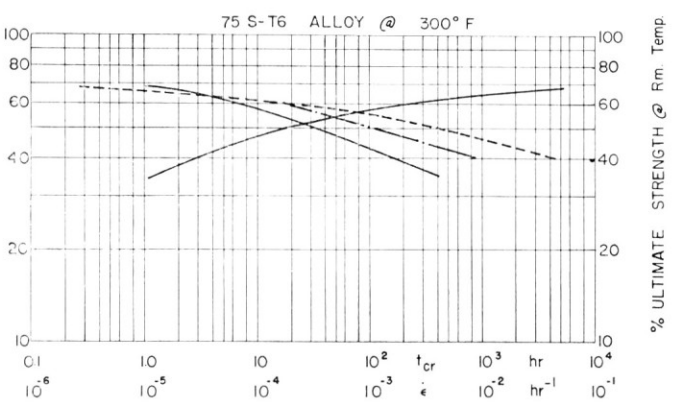

FIG. 5. Steady creep rate and rupture time.

Of course, the metallographic structure of the 75S-T6 material changes when the specimen is exposed to high temperatures. One indication of this change is the decrease of static tensile strength with time of exposure. According to Ref. 5, the ultimate stress after 10^4 hours of exposure may be as low as one-third of the value observed after $\frac{1}{2}$ hr of exposure.

To improve the agreement, a trial-and-error process was devised in which the ultimate stress was assumed first and the integration extended from σ_0 to σ_u to obtain the critical time; subsequently a modified value of σ_u was assumed to agree with the experimental value corresponding to t_{cr}. When this procedure was continued until a consistent set of values was obtained, the results were in considerably better agreement with experiment than the original critical times. The improved theoretical values are shown by the dash-dotted lines. These lines still differ from the experimental curves but the effect of prolonged heating on the creep properties of the material could not be taken into account in a satisfactory manner because of lack of information.

The first two figures contain data from a paper by Sherby and Dorn[4] while the experimental curves of the last two figures were taken from the ANC–5 bulletin[5].

C. Application to Various Creep Laws

1. *Power law.* When the creep law is

$$\dot{\epsilon} = f(\sigma) = (\sigma/\lambda)^n \tag{19}$$

substitution of $\sigma = \sigma_0 R$ gives

$$f(\sigma) = f(\sigma_0 R) = (\sigma_0 R/\lambda)^n \tag{20}$$

and equation (16) can be written in the form

$$t_{cr} \simeq \int_1^\infty \frac{dR}{Rf(\sigma_0 R)} = \int_1^\infty \frac{dR}{(\sigma_0/\lambda)^n R^{n+1}} \tag{21}$$

Integration and substitution of the limits yield

$$t_{cr} \simeq \frac{1}{n(\sigma_0/\lambda)^n} = 1/(n\dot{\epsilon}_0) \tag{22}$$

where $\dot{\epsilon}_0$ is the nominal strain rate, that is the strain rate obtainable from equation (19) upon substitution of the nominal stress $\sigma_0 = P/A_0$. This very simple formula was derived in Ref. 2.

In some cases it may be necessary to distinguish between the correct upper limit of R, namely σ_u/σ_0, and infinity. With the correct upper limit the critical time becomes

$$t_{cr} = \frac{1}{n\dot{\epsilon}_0}\left[1 - \left(\frac{\sigma_0}{\sigma_u}\right)^n\right] = \frac{1}{n}\left[\frac{1}{\dot{\epsilon}_0} - \frac{1}{\dot{\epsilon}_u}\right] \tag{23}$$

where $\dot{\epsilon}_u$ is the creep rate obtainable from equation (19) upon substitution of σ_u for σ.

It follows from equation (22) that

$$t_{cr}\dot{\epsilon}_0 \simeq 1/n \tag{24}$$

Even though equation (24) was proved in Ref. 2 in 1953, there are still statements in the literature (see, for instance, Refs. 6, 7, and 8) to the effect that

$$t_{cr}\dot{\epsilon}_0 = C = \text{const.} \tag{25}$$

is an empirical law. Granted that equations (22) to (24) were derived only for the power law, while equation (25) has been observed to be approximately true even in cases when the power law did not hold. As both the creep rate and the critical time are usually plotted along the axis of abscissas according to a logarithmic scale while the corresponding stress is measured along the axis of ordinates either according to a Cartesian or to a logarithmic scale, equation (25) implies that the strain rate and critical time curves are symmetric with respect to a vertical straight line whose abscissa is $(\frac{1}{2}) \log C$. This follows immediately from equation (25) if logarithms are taken:

$$\log t_{cr} + \log \dot{\epsilon}_0 = \log C \tag{26}$$

When the power law of creep and equation (24) hold, the two curves are straight lines.

It is of some interest to prove that the only steady creep law that can lead to equation (25), if the physical assumptions made in the derivations of this section are maintained and if infinity is taken as the upper limit of the integral, is indeed the power law. Equation (18) can be re-written as

$$t_{cr} = \int_{\sigma_0}^{\infty} \frac{d(\log \sigma)}{f(\sigma)} = \int_{\sigma_0}^{\infty} \frac{d\sigma}{\sigma f(\sigma)} \tag{27}$$

This is the critical time corresponding to the nominal stress σ_0. At the same stress the strain rate is $\dot{\epsilon}_0 = f(\sigma)$. The constancy of the product is expressed, therefore, by

$$f(\sigma_0) \int_{\sigma_0}^{\infty} \frac{d\sigma}{\sigma f(\sigma)} = K = \text{const.} \tag{28}$$

This can also be written as

$$\int_{\sigma_0}^{\infty} \frac{d\sigma}{\sigma f(\sigma)} = \frac{K}{f(\sigma_0)} \tag{29}$$

A variation of the lower limit of the definite integral yields

$$\frac{-d\sigma_0}{\sigma_0 f(\sigma_0)} = \frac{-Kf'(\sigma_0)\, d\sigma_0}{[f(\sigma_0)]^2} \tag{30}$$

where the prime denotes differentiation with respect to σ_0. This becomes after shortening and rearranging

$$y' - (1/Kx)y = 0 \tag{31}$$

If the following notation is used:

$$x = \sigma_0 \qquad y = f(\sigma_0) = f(x) \tag{32}$$

In equation (31) the variables are separable:

$$\frac{dy}{y} = \frac{1}{K}\frac{dx}{x} \tag{33}$$

The integral is

$$y = Cx^{1/K} \tag{34}$$

which is the power law.

2. *Exponential law.* When the creep strain rate is governed by the exponential law

$$\dot{\epsilon} = ke^{\sigma/s} = f(\sigma) \tag{35}$$

where k and s are constants to be determined from experiment, substitution in equation (27) gives

$$t_{cr} = \int_{\sigma_0}^{\infty} \frac{e^{-\sigma/s}\,d\sigma}{k\sigma} = \frac{1}{k}\int_{\sigma_0/s}^{\infty} \frac{e^{-\sigma/s}\,d(\sigma/s)}{\sigma/s} \tag{36}$$

The indefinite integral can be evaluated by integrations by parts:

$$I = \int e^{-y}y^{-1}\,dy = -e^{-y}\left[\frac{1}{y} - \frac{1}{y^2} + \frac{2}{y^3} - \frac{6}{y^4} + \dots\right] \tag{37}$$

The series in brackets is an asymptotic series. If it is broken off after the nth term, the maximum possible error committed is the value of the $(n+1)$th term[9]. The approximate value of the critical time is then

$$t_{cr} \simeq \exp(-\sigma_0/s)(s/\sigma_0 k)[1 - (s/\sigma_0) + 2(s/\sigma_0)^2 - 6(s/\sigma_0)^3 + \dots] \tag{38}$$

A more accurate value is

$$\begin{aligned} t_{cr} = {} & \exp(-\sigma_0/s)(s/\sigma_0 k)[1 - (s/\sigma_0) + 2(s/\sigma_0)^2 - 6(s/\sigma_0)^3 + \dots] \\ & - \exp(-\sigma_u/s)(s/\sigma_u k)[1 - (s/\sigma_u) + 2(s/\sigma_u)^2 - 6(s/\sigma_u)^3 + \dots] \end{aligned} \tag{39}$$

where σ_u is the ultimate tensile stress of the material at the test temperature.

As the value of σ_0/s is likely to range between 2 and 20 in aeronautical applications, and σ_u/s is usually larger than σ_0/s by a factor of 2 to 10, a good approximation can often be had by writing

$$t_{cr} \simeq (1/k)\exp(-\sigma_0/s)(s/\sigma_0) = s/\sigma_0\dot{\epsilon}_0 \tag{40}$$

The percentage error committed when this formula is used should not be much greater than 100 (s/σ_0).

A slightly more accurate expression is

$$t_{cr} = s\left[\frac{1}{\sigma_0\dot{\epsilon}_0} - \frac{1}{\sigma_u\dot{\epsilon}_u}\right] \tag{41}$$

When σ_0/s is comparatively small, say, smaller than 3, the above approach may be too inaccurate or too inconvenient. One can then make use of tables of the exponential integral defined as

$$-\mathrm{Ei}(-x) = \int_x^\infty e^{-y}y^{-1}\,dy \tag{42}$$

This function is tabulated, for instance, on p. 6 of Ref. 10. Substitution in equation (36) gives

$$t_{cr} \simeq -(1/k)[\mathrm{Ei}(-\sigma_0/s)] \tag{43}$$

With the more accurate upper limit one has

$$t_{cr} = -(1/k)[\mathrm{Ei}(-\sigma_0/s) - \mathrm{Ei}(-\sigma_u/s)] \tag{44}$$

3. *Primary creep law.* When the results of constant-stress creep tests can be represented by the primary creep law

$$\epsilon = g(\sigma)\,t^{1/m} \tag{45}$$

assumption of the existence of a mechanical equation of state yields the following expression which is valid for variable stresses also[3]:

$$\dot{\epsilon} = (1/m)[g(\sigma)]^m\epsilon^{1-m} \tag{46}$$

If this law is generalized further to hold for large deformations through substitution of $\log R$ for ϵ and $\sigma_0 R$ for σ, the result is

$$(\mathrm{d}/\mathrm{d}t)\log R = (1/R)(\mathrm{d}R/\mathrm{d}t) = (1/m)[g(\sigma_0 R)]^m(\log R)^{1-m} \tag{47}$$

If it is now assumed that the function

$$g(\sigma) = (\sigma/\lambda)^n \tag{48}$$

and the variables are separated in equation (47), one obtains

$$\mathrm{d}t = m(\lambda/\sigma_0)^{mn}(1/R)^{mn+1}(\log R)^{m-1}\,\mathrm{d}R \tag{49}$$

The substitution

$$R = e^x \tag{50}$$

changes this equation over into

$$\mathrm{d}t = m(\lambda/\sigma_0)^{mn}e^{-mnx}x^{m-1}\,\mathrm{d}x \tag{51}$$

The critical time is then

$$t_{cr} = m(\lambda/\sigma_0)^{mn}\int_0^{\log(\sigma_u/\sigma_0)} x^{m-1}e^{-mnx}\,\mathrm{d}x \tag{52}$$

When p is a positive integer, the indefinite integral

$$\int x^p e^{-ax}\,\mathrm{d}x = -e^{-ax}\left[\frac{x^p}{a} + \frac{px^{p-1}}{a^2} + \frac{p(p-1)x^{p-2}}{a^3} + \ldots + \frac{p!}{a^{p+1}}\right] \tag{53}$$

If this expression is used in the evaluation of the critical time, in the lower limit only the last term in brackets remains. Moreover, the upper

limit vanishes completely if, in an approximate manner, the upper limit is replaced by infinity. Under these conditions equation (52) becomes

$$t_{cr} \simeq [m!/(mn)^m](\lambda/\sigma_0)^{mn} \tag{54}$$

where the exclamation mark indicates the factorial function. For particular values of m this expression reduces to

$$t_{cr} \simeq (1/n)(\lambda/\sigma_0)^n \quad \text{when } m = 1 \tag{55a}$$

$$t_{cr} \simeq (1/2)(1/n)^2(\lambda/\sigma_0)^{2n} \quad \text{when } m = 2 \tag{55b}$$

$$t_{cr} \simeq (2/9)(1/n)^3(\lambda/\sigma_0)^{3n} \quad \text{when } m = 3 \tag{55c}$$

$$t_{cr} \simeq (3/32)(1/n)^4(\lambda/\sigma_0)^{4n} \quad \text{when } m = 4 \tag{55d}$$

When m is not an integer, the substitution

$$mnx = s \tag{56}$$

transforms equation (52) into

$$t_{cr} = [m/(mn)^m](\lambda/\sigma_0)^{mn} \int_0^{mn \log (\sigma_u/\sigma_0)} e^{-s} s^{m-1}\, ds \tag{57}$$

When the upper limit is taken in an approximate manner as infinity, the equation reduces to

$$t_{cr} = [m/(mn)^m](\lambda/\sigma_0)^{mn}\Gamma(m) \tag{58}$$

where $\Gamma(m)$ is the gamma function tabulated, for instance, in Ref. 10.

With the exact upper limit one has

$$t_{cr} = [m/(mn)^m](\lambda/\sigma_0)^{mn}\{\Gamma(m) - \Gamma[m, mn \log (\sigma_u/\sigma_0)]\} \tag{59}$$

where

$$\Gamma[m, mn \log (\sigma_u/\sigma_0)] = \int_{mn \log (\sigma_u/\sigma_0)}^{\infty} e^{-s} s^{m-1}\, ds \tag{60}$$

is the incomplete gamma function.

3. CREEP BUCKLING

A. The Buckling Process

Just as a bar subjected to tension fails after a finite time when its material creeps, so does a column in the presence of creep when it is under the action of a compressive load P, however small. This mode of failure of the column is known as creep buckling. Even though creep buckling was first described in the technical literature only a dozen years ago, a number of different processes have already been proposed to explain the phenomenon. They were reviewed in detail by the author in a recent publication[11] which contains a reasonably complete bibliography of the subject. For this reason references to the history of creep buckling theory are not given here; the purpose of this article is to present one particular approach to the analysis of creep buckling which, in the author's opinion, is in the best agreement with observations made in creep-buckling tests carried out with metal columns at high temperatures. This approach was developed jointly by B. Fraeijs de Veubeke[12] and the author.

It is self-evident that every column is imperfect; because of the inaccuracies of the manufacturing process and of the alignment in the testing machine, its centerline deviates from the straight line along which the compressive load is acting. The product of force and deviation is a bending moment under the action of which the initial curvature of the column increases with time in consequence of creep. The increases in curvature take place very slowly at the outset if the column is carefully machined and centered and if the applied load is substantially smaller than the Euler load. After a while the velocity of lateral deflection increases and the column collapses quite suddenly when a critical value of the lateral deflection is reached.

B. Flexural Rigidity of Deflected Column

The reason for sudden buckling at the critical deflection can be understood if the variations in the flexural rigidity of the column with increasing deflection are investigated. To simplify the analysis, let us assume that the cross-section of the column consists of two concentrated flanges, each of an area $A/2$, which are held a distance h apart by a web which has no resistance to normal stresses but is perfectly rigid in shear. This approximation to reality has been shown to be an excellent one in the case of I-sections and for many purposes it is satisfactory even with solid rectangular sections.

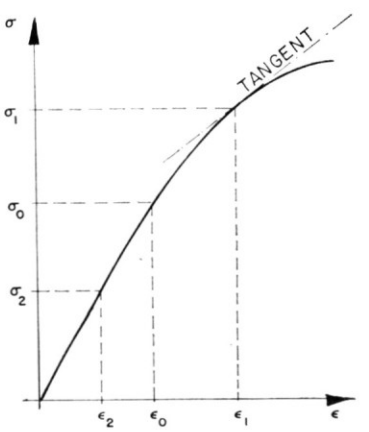

FIG. 6. Stress–strain diagram of material.

The stress-strain curve of the material is shown in Fig. 6; it should represent the behavior of the material at the moment of collapse which may differ considerably from the behavior at the beginning of the creep buckling test. The change in material properties is due largely to the exposure to the high temperature; the effect of the creep deformation is

usually negligible since in aeronautical applications the maximum strain just before collapse is generally of the order of the Euler strain

$$\epsilon_E = \pi^2/(L/\rho)^2 \tag{61}$$

where L is the length of the pin-ended column and ρ is the radius of gyration of the cross-section. If the slenderness ratio L/ρ is 50, the Euler strain is about 0·4%. The effect of such a small creep strain on the instantaneous response of the material to loading can safely be disregarded.

At the moment of load application the stress in the two flanges is the same for all practical purposes if the initial deviations from straightness are very small. It is

$$\sigma_0 = P/A \tag{62}$$

As the deviations increase in consequence of creep, the stress σ_1 in the concave flange increases and the stress σ_2 in the convex flange decreases. After a while the values of σ_1 and σ_2 may be as indicated in Fig. 6; the increase in σ_1 must be equal in absolute value to the decrease in σ_2 because the load P is constant.

If we wish to test the flexural rigidity of the column, we can increase by an infinitesimal amount the amplitude of the lateral deflections and calculate the corresponding change in the bending moment. The increase in curvature is

$$(\Delta\epsilon_1 - \Delta\epsilon_2)/h = \Delta\kappa \tag{63}$$

where the strain is positive if it is compressive. The increment in the compressive stress on the concave side of the column is

$$\Delta\sigma_1 = E_t\Delta\epsilon_1 \tag{64}$$

where the tangent modulus E_t is the slope of the tangent to the stress strain curve at point C. The change in the stress in the flange on the convex side is

$$\Delta\sigma_2 = E\Delta\epsilon_2 \tag{65}$$

which is a negative quantity as $\Delta\epsilon_2$ is negative indicating a diminishing of the compressive strain. In this equation E is Young's modulus; it must be used when the stress decreases because only the elastic part of the deformations can be regained. For reasons of equilibrium

$$(\Delta\sigma_1 + \Delta\sigma_2)(A/2) = \Delta P = 0 \tag{66}$$

The increase in bending moment is therefore

$$\Delta M = \Delta\sigma_1(A/2)h = -\Delta\sigma_2(A/2)h \tag{67}$$

By definition, the effective bending rigidity $(EI)_{\text{eff}}$ is the increment in bending moment divided by the increment in curvature:

$$(EI)_{\text{eff}} = \frac{\Delta\sigma_1(A/2)h}{(\Delta\epsilon_1 - \Delta\epsilon_2)/h} \tag{68}$$

Substitutions yield

$$(EI)_{\text{eff}} = E_{\text{eff}}I = \frac{2EE_t}{E + E_t}\frac{Ah^2}{4} \tag{69}$$

where I is the moment of inertia of the idealized I-section.

If the initial value σ_0 of the stress at the moment of load application is less than the elastic limit of the material, the initial bending rigidity of the column is

$$(EI)_0 = E(Ah^2/4) \tag{70}$$

Equation (69) reduces to this value if E is substituted for E_t. If the initial value σ_0 of the stress exceeds the elastic limit, E_t in equation (69) has to be determined from the slope of the tangent corresponding to σ_0. The effective bending rigidity so obtained was proposed for use in buckling calculations by von Kármán in 1910[13].

As the column deflects further and further under the influence of creep, its instantaneous bending rigidity also decreases since E_t in equation (69) decreases. If this value were the same along the entire column, the buckling load would be

$$P_{cr} = \pi^2(EI)_{eff}L^2 \tag{71}$$

where L is the length of the column. Correspondingly the critical value of the average stress would be

$$\sigma_{0.cr} = P_{cr}/A = \pi^2 E_{eff}/(L/\rho)^2 = \epsilon_E E_{eff} \tag{72}$$

where ϵ_E is the Euler strain defined in equation (61) and ρ is the radius of gyration of the section:

$$\rho = h/2 \tag{73}$$

Since the value of E_t is least at the middle of the column where the curvature, and consequently the stress, is highest, equation (71) is a conservative estimate of the buckling load.

The interesting situation arises, therefore, that the critical value of the average stress $\sigma_{0,cr}$ decreases as the amplitude of the lateral deflections increases while the average stress $\sigma_0 = P/A$ remains constant. When the critical value of the deflection is reached, $\sigma_{0,cr} = \sigma_0$, and the column suddenly buckles.

C. Calculation of the Critical Deflection

The critical value of the lateral deflection amplitude depends only on the stress-strain curve, the slenderness ratio of the column, the value of the applied load P (or applied stress $\sigma_0 = P/A$) and the deflected shape of the column, but it is independent of the creep characteristics of the material. It will now be calculated on the assumption that both the initial shape of deviations and the deflected shape can be approximated by a half sine wave. This was proved to be permissible under most conditions of interest in aircraft structural applications. Moreover, the conditions of equilibrium and deformation will be enforced only at the middle of the column. A more general analysis, making use of Fourier series, is possible but much more complicated. In all those cases in which comparisons are available, the so-called one-point collocation method and the more rigorous analysis yield results that differ relatively little[14].

If the deflection of the midpoint of the column is $a\rho$ where a is the non-dimensional deflection amplitude, the stress in the concave flange is

$$\sigma_1 = \frac{P}{A} + \frac{M}{(A/2)h} = \frac{P}{A} + \frac{Pa\rho}{A(h/2)} = \sigma_0(1 + a) \tag{74}$$

Hence for a given value of the applied stress σ_0 the critical value of the non-dimensional deflection amplitude is

$$a_{cr} = (\sigma_1/\sigma_0) - 1 \tag{75}$$

At the same time one must also satisfy the buckling condition

$$\sigma_0 = \epsilon_E E_{eff} \tag{76}$$

where E_{eff} is a uniquely-defined function of σ_1.

If the stress–strain curve is known, the following procedure is convenient for the establishment of the relationship between applied stress σ_0 and critical non-dimensional deflection amplitude a_{cr}:

(1) Assume a value ofσ_1.
(2) Determine the corresponding E_t from the stress–strain curve.
(3) Calculate E_{eff} from equation (69).
(4) Establish the relationship between σ_1 and E_{eff} for the entire range of stress of interest.
(5) From the known geometry of the column compute ϵ_E from equation (61).
(6) Substitute ϵ_E and a selected value of E_{eff} in equation (76) to obtain the average stress σ_0.
(7) Substitute this value of σ_0 and the value of σ_1 corresponding to the selected value of E_{eff} in equation (75) to obtain a_{cr}.
(8) Plot these values of a_{cr} against the σ_0 values of (7); the curve is the relationship required for the prescribed geometry and material properties.

D. Use of the Ramberg–Osgood Relationship

At room temperature the stress-strain curve of the material can usually be approximated by the following expression[15]:

$$\epsilon = (\sigma/E) + (\sigma/B)^p \tag{77}$$

It will now be assumed that this is an accurate enough approximation at high temperatures also. The tangent modulus value is then

$$E_t = d\sigma/d\epsilon = 1/(d\epsilon/d\sigma) = [(1/E) + (p/B)(\sigma_1/B)^{p-1}]^{-1} \tag{78}$$

The subscript 1 under the σ indicates that E_t has to be calculated for the value of the compressive stress prevailing in the concave flange. From equation (69) the effective modulus is

$$E_{eff} = E[1 + (p/2)(E/B)(\sigma_1/B)^{p-1}]^{-1} \tag{79}$$

From equation (76) one obtains

$$\sigma_0 = \sigma_E[1 + (p/2(E/B)(\sigma_1/B)^{p-1}]^{-1} \tag{80}$$

With the aid of this expression equation (75) yields

$$a_{cr} = (1/\sigma_E)[\sigma_1 + (p/2)E(\sigma_1/B)^p] - 1 \tag{81}$$

But equation (75) can also be solved for σ_0 to give

$$\sigma_0 = \sigma_1/(1 + a_{cr}) \tag{82}$$

When the geometry of the column and the stress–strain curve of the material are given, E, p, B, and σ_E are known. Substitution of a selected value of σ_1 in equation (81) yields the value of a_{cr}. Substitution of this value in equation (82) gives the corresponding value of σ_0.

E. Calculation of the Critical Time

When the critical value of the non-dimensional deflection amplitude as well as its initial value is known, the critical time can be obtained without difficulty provided that sufficient information is available on the creep behavior of the material. Let a_{00} denote the initial non-dimensional amplitude of the deviations from straightness before load application; it was shown in Ref. 11 that a half sine wave represents the distribution of the deviations along the axis with sufficient accuracy for the present purposes. The application of the load P causes an instantaneous elastic increment in this amplitude; the increased value a_0 can be computed from the formula

$$a_0 = a_{00}/[1 - (P/P_E)] \tag{83}$$

where P_E is the Euler load of the column. When the stress exceeds the elastic limit of the material, an additional instantaneous plastic deformation also takes place. The magnitude of this deformation was calculated in Refs. 16 and 17.

The creep process begins immediately upon load application. As was shown, for instance, in Ref. 18, the rate of change of a is given by

$$\dot{a} = (1/2\epsilon_E)(\dot{\epsilon}_1 - \dot{\epsilon}_2) \tag{84}$$

Consequently the critical time is

$$t_{cr} = 2\epsilon_E \int_{a_0}^{a_{cr}} da/(\dot{\epsilon}_1 - \dot{\epsilon}_2) \tag{85}$$

When the creep law is

$$\dot{\epsilon} = (\sigma/\lambda)^n \tag{86}$$

equation (85) becomes

$$t_{cr} = \frac{2\epsilon_E}{\dot{\epsilon}_0} \int_{a_0}^{a_{cr}} \frac{da}{(1 + a)^n - (1 - a)^n} \tag{87}$$

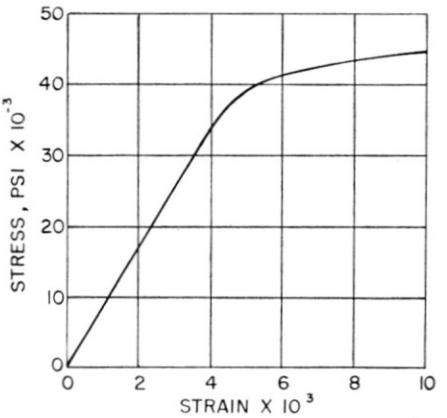

FIG. 7. Stress–strain curve for 2024–T4 Al. alloy at 500°F (from Ref. 17).

F. Numerical Example

The theory will now be illustrated with a numerical example in which the critical time of a column will be calculated. The stress–strain curve of instantaneous loading is given in Fig. 7; it was taken from Ref. 17. It represents the behavior of 2024–T4 aluminum alloy at 500°F. In accordance with the Ramberg–Osgood approach[15], the curve will be approximated by the formula

$$\epsilon = (\sigma/E) + (\sigma/57{,}800)^{20} \tag{88}$$

As the experiments described in Ref. 17 were made with columns of a slenderness ratio of 52·7, this value will be taken here also. With a cross-sectional area of

$$A = \tfrac{1}{8}\ \text{in.}^2 \tag{89}$$

and a modulus value determined from Fig. 7 as

$$E = 8{\cdot}55 \times 10^6\ \text{psi} \tag{90}$$

the following quantities can be computed:

$$\epsilon_E = 0{\cdot}00356 \qquad \sigma_E = 30{,}400\ \text{psi} \qquad P_E = 3800\ \text{lb} \tag{91}$$

With the aid of these values the connection between applied load P and critical non-dimensional deflection amplitude a_{cr} can be calculated from equations (81) and (82). The results are plotted in Fig. 8; they agree very well with those obtained in Ref. 17 with the aid of a graphical-numerical procedure.

It is of interest to note that a_{cr} is less than 2, that is, buckling takes place before the maximum lateral deflection reaches a value equal to the depth h of the idealized section, if the load exceeds 43·5% of the instantaneous buckling load. Such a high percentage is common in aircraft and missile structural testing while in stationary powerplant tests the percentage is usually lower.

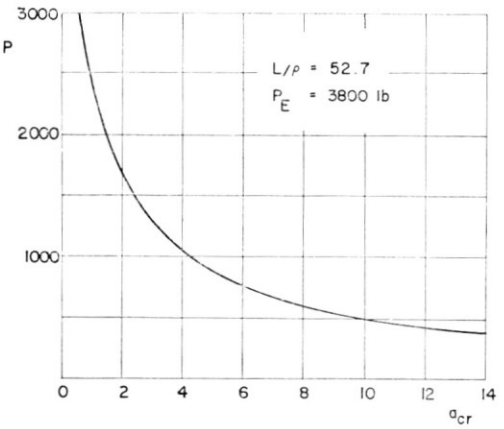

FIG. 8. Critical non-dimensional deflection as function of applied load.

Next the creep behavior of the material was investigated. It was not found possible to represent with a satisfactory degree of accuracy the creep curves published by a power-function type steady creep law. Nevertheless the formula

$$\dot{\epsilon} = (\sigma/248{,}000)^4 \tag{92}$$

was adopted for the analysis as it permits the development of closed-form

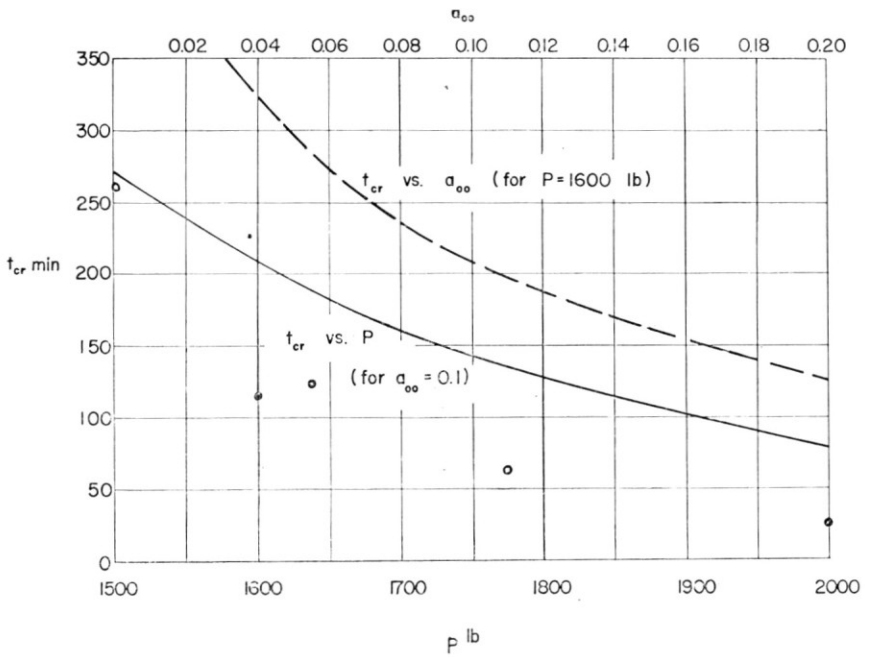

FIG. 9. Critical time of column.

solutions. After the substitution of $n = 4$ in equation (87) the integration was carried out with the result that

$$t_{cr} = \frac{1}{8}\frac{\epsilon_E}{\dot{\epsilon}_0}\log\frac{1+(1/a_0)^2}{1+(1/a_{cr})^2} \tag{93}$$

This equation was used first to evaluate the effect of changes in the initial deviations. Values of a_{00} were assumed and substituted in equation (83) to obtain a_0; these in turn were substituted in equation (93) to obtain t_{cr}. The load was assumed as 1600 lb. The results are plotted in the dotted curve of Fig. 9.

Finally the effect of changes in the applied load P was investigated. For each value of the load the corresponding values of $\dot{\epsilon}_0$ and a_{cr} were substituted in equation (93) with a_{00} taken as 0·1. The results are shown in Fig. 9 by the full line.

A few remarks of interest can be made in connection with Fig. 9. First the overwhelming effect of the load on the critical time is evident. A change by a factor of about 3·5 in lifetime was achieved through a change in load by a factor of 1·33. In comparison, for a change in lifetime by a factor of about 2·8 a change in initial deviation amplitude by a factor of 6·66 is required.

The circles in the diagram are the experimental points corresponding to the full line. At $P = 1500$ lb the agreement between theory and experiment is good, but at higher loads the experimental lifetime is only about half the theoretical value. It may be mentioned that this is not considered a bad disagreement in creep investigations where the scatter of the results is always great. But of course in the present analysis great accuracy could not be expected because the empirical formula of equation (92) fits the test data poorly. It should also be noticed that the percentage deviation is much smaller if it is based on allowable load values for a prescribed lifetime. For instance, a lifetime of 120 hr can be achieved if the load is 1825 lb according to the curve, or 1625 lb according to the experimental points.

4. HEAT SINKS AND ABLATION

A. Background Information

The most radical departure from classical design methods can be observed with re-entry vehicles. They include the ballistic missile whose nose cone has already been successfully recovered on a few occasions; shuttle vehicles to satellites; and space ships designed to descend on the Earth or on some other planet, which, of course, have yet to be built. The main problem with these new types of craft is how to take care of the very large amount of heat flowing into the structure from the boundary layer of air during the decelerating phase of the flight. A number of proposals have been made by designers to overcome this difficulty.

Perhaps the simplest method already tried is the incorporation of a sufficient amount of heat capacity in the structural elements of the vehicle to absorb the heat without an undue deterioration of the material. Such a structure acts as a heat sink. The material may retain enough strength, in spite of the high temperature reached, to withstand the pressure and inertia loads imposed upon it. Alternatively, it may be backed up by a cooler and stronger material which is called upon to maintain the structural integrity of the vehicle.

One step further removed from airplane design practice is the structure that is covered with a layer of material destined to be used up during flight. The removal—or ablation—of this layer can be initiated by melting, vaporization, sublimation, or burning. The contribution of the ablation process to the protection of the structure below the expendable material is threefold; the layer absorbs heat as its temperature is raised; it absorbs heat during phase changes; and it modifies the flow in the boundary layer in a manner that decreases the heat input in the structure.

Exact analyses of these processes are difficult because of their inherent nonlinearity and because of the many variables involved. A great deal of effort is now being spent in the United States to clarify the basic physical facts and to develop numerical methods for analyzing individual designs. The most important quantity to be calculated is the lifetime of the structure.

A few comparatively simple considerations relative to these processes are presented in the next few articles.

B. Heat Sink

When the surface of a missile re-entering the atmosphere is subjected to very rapid heating for a very short time, the structure can absorb the heat if its material has a high thermal capacity and a high conductivity. The latter is just as important as the former because, in a poor conductor, the heat must be absorbed in a very thin layer of the material near the heated surface and the rest of the thickness cannot contribute to the storage of heat.

The relative merits of different materials can be easily established in a first approximation if a number of rather far-reaching simplifying assumptions are made. The heat flow into the structure will be assumed constant during the heating period; similarly constant average values will be introduced in the heat flow equation for conductivity, specific heat and specific weight. One-dimensional heat flow alone will be taken into account; this means that the wall will be considered a flat slab of large dimensions subjected to uniform heating over one surface. It will also be assumed that the conditions at the inner surface of the wall have no noticeable effect on the temperature distribution; this is equivalent to saying that the wall is infinitely thick.

This highly-simplified problem can be characterized mathematically in the following manner:

$$\partial\Phi/\partial t = a(\partial^2\Phi/\partial x^2) \qquad x > 0 \qquad t > 0 \tag{94a}$$

$$\Phi = 0 \qquad t = 0 \qquad x > 0 \tag{94b}$$

$$\Phi = C \qquad x = 0 \qquad t > 0 \tag{94c}$$

In these equations

$$\Phi = -K(\partial T/\partial x) \tag{95}$$

is the heat flux, C its prescribed constant value at the boundary (the heating rate), K the thermal conductivity, x the distance measured from, and perpendicular to, the heated surface, t the time counted from the beginning of the heating, and a the thermal diffusivity defined by the equation

$$a = K/c\rho \tag{96}$$

with c the specific heat and ρ the density. If the uniform initial temperature is T_0, integration of this boundary value problem yields

$$T - T_0 = (2C/K)(at)^{1/2}\,\text{ierfc}\,[x/2\sqrt{(at)}] \tag{97}$$

where ierfc denotes the iterated complementary error function defined in Ref. 19. Since

$$\text{ierfc}\,(0) = 1/\sqrt{\pi} \tag{98}$$

the surface temperature can be given as

$$(T - T_0)_{x=0} = (2C/K)(at/\pi)^{1/2} \tag{99}$$

The equation shows that the surface temperature increases as the square root of time when the heat flux into the structure is constant.

The suitability of a material to act as a heat sink will now be judged on the basis of the time t_m necessary to melt the surface. Equation (99) can be solved for t_m after substitution of T_m of $T_{x=0}$ and t_m for t. One obtains

$$t_m = (\pi/4a)(K/C)^2(T_m - T_0)^2 \tag{100}$$

If T_0 is taken as 400°R, C as 1000BTU/ft² sec, and the values of a, K, and T_m are substituted into the formula from Table I, one obtains the melting time values listed in the next to the last row of the table.

It is to be noted that graphite does not melt, but sublimes. Hence in the case of graphite T_m is the sublimation temperature.

The table shows that a heating time of 6 sec can be withstood by copper, beryllium, and graphite, but not by Inconel-X in spite of its high melting temperature. The trouble lies, of course, in the low conductivity and the low heat capacity of this material. The slow penetration of heat into the Inconel-X slab as compared to the other slabs can be seen if one calculates the distance $x_{1/4}$ at which the temperature is one-quarter of the melting temperature.

TABLE 1

Melting time t_m for constant heat flux C = 1000 BTU/ft² sec

	Copper	Beryllium	Inconel-X	Graphite
c, BTU/lb°R	0·105	0·66	0·13	0·5
K, BTU/hr ft°R	205	65	11	25
T_m, °R	2442	2805	3030	7060
ρ, lb/in³	0·322	0·067	0·307	0·081
a, in²/min	8·42	2·04	0·38	0·86
t_m, sec	10·9	6·26	1·15	16·9
$x_{\frac{1}{4}}$ in.	1·58	0·59	0·11	0·63

For any given material and at any given time the temperature distribution through the slab depends on the function ierfc$[x/2\sqrt{(at)}]$. The value of this function [19] is $1/\sqrt{\pi}$ when the argument is zero, and one-quarter of this value, that is 0·141, when the argument is 0·64.

Consequently

$$x_{1/4}/2\sqrt{(at_m)} = 0{\cdot}64 \tag{101}$$

from which the distance follows as

$$x_{1/4} = 1{\cdot}28\sqrt{(at_m)} \tag{102}$$

Values of $x_{1/4}$ computed from equation (102) are entered in the last row of Table I. They show that the penetration depth for Inconel-X is only 0·11 in. It can also be seen from the table that a one-inch thick slab can be considered as an infinitely thick one for most practical purposes, up to the time when the heated surface begins to melt, if the material is beryllium or graphite. With copper this is not quite true, but the slab can be considered infinitely thick in a rough approximation up to 6 sec of heating. Indeed at that time the maximum temperature is 1913°R and $x_{1/4}$ is 1·175 in.

If the heating period lasts 6 sec only, the structure can be built of copper, beryllium or graphite. The former two must be close to one inch thick; hence beryllium is preferable because it weighs only about one-fifth as much as copper. Graphite would be even better although its density is about 20% higher than that of beryllium. On the other hand, a graphite structural element could be made considerably thinner than one inch if the heating lasted only 6 sec.

A much more accurate analysis of the behavior of a heat sink was carried out recently by Stalder[20]. The heating rate was assumed in accordance with the flight path of a nose cone characterized by $W/C_D A = 345$ re-entering the atmosphere at a speed of 23,000 ft/sec. Here W is the weight, C_D the drag coefficient, and A the frontal area of the nose cone. The variation of the external heat transfer coefficient h and of the recovery temperature T_r is shown in Fig. 10.

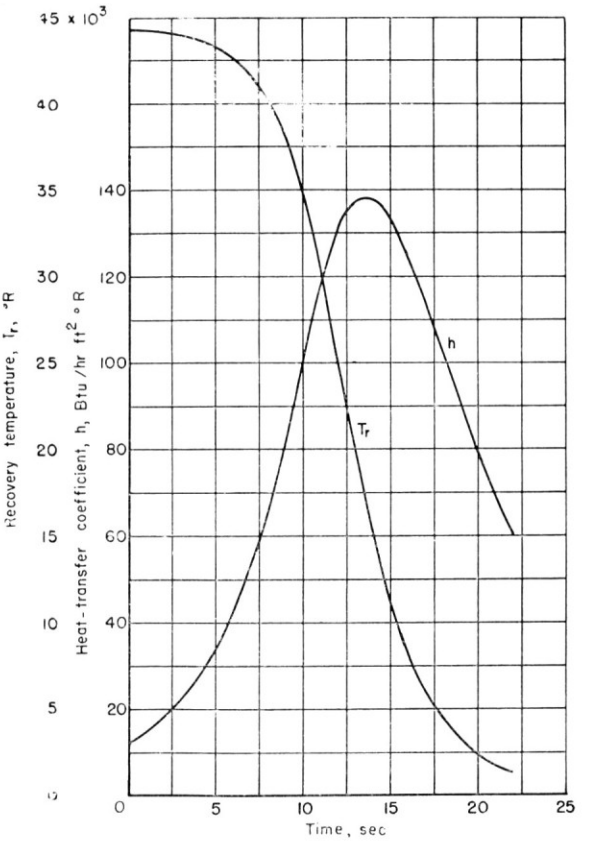

FIG. 10. Heating characteristics of re-entry body.
(from Ref. 20)

As the thermal properties of the structural materials vary significantly between ambient temperature and the melting temperature, the variation was duly considered in the calculation. As an example for this variation the values of K and c are plotted in Fig. 11 as functions of the temperature. Finally, the assumption of an infinite thickness was abandoned and the actual thickness b was included in the analysis; at $x = b$ the wall was assumed to be insulated.

The resulting mathematical statement of the problem is:

$$\rho c(\partial T/\partial t) = (\partial/\partial x)[K(\partial T/\partial x)] \tag{103a}$$

$$x = b \qquad \partial T(b, t)/\partial x = 0 \qquad t > 0 \tag{103b}$$

$$x = 0 \qquad K[\partial T(0, t)/\partial x] = h[T_r - T(0, t)] - \epsilon\sigma T^4(0, t) \tag{103c}$$

$$T = 400°\text{R} \qquad 0 < x < b \qquad t = 0 \tag{103d}$$

Here ϵ, the emissivity, was taken as 0·7 and σ is Boltzmann's radiation constant.

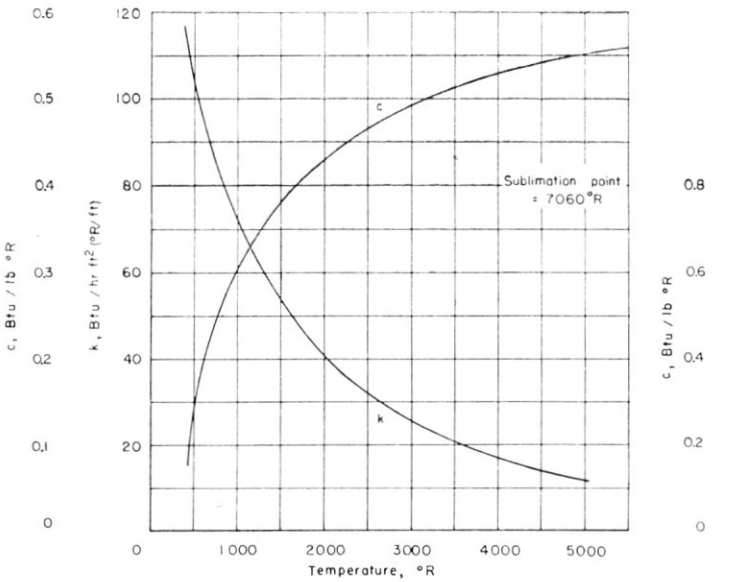

FIG. 11. Variation of conductivity and specific heat of graphite with time. (from Ref. 20)

Numerical integration of the differential equation showed a very large influence of the variability of the thermal properties of the material on the temperatures in the wall in the case of graphite, and considerably less of an effect in the case of copper. With graphite the maximum temperature reached in the heating process was found to be 3460°R when average values were used, as compared with 2200°R obtained when the variability was taken into account.

Some of the results of the calculations are shown in Fig. 12. They are the temperatures of the heated surface and of the insulated surface when the two are one inch apart, as well as the total heat Q transferred through one square foot of the surface, with the three quantities plotted against time. The material of construction is graphite.

An interesting conclusion was drawn by Stalder from the results of his numerical integrations. He found that the external heating history prescribed caused a maximum wall temperature just equal to the melting or sublimation temperature, if the wall thickness was about $\frac{1}{4}$, $1\frac{3}{4}$, and 2 in. for graphite, beryllium, and copper, respectively. The total heat absorbed by one pound of each material was 1980, 534, and 84 BTU. Hence theoretically the graphite wall could be built to weigh about one-twenty-fourth, and the beryllium wall one-sixth as much as the copper wall.

Of course, considerations other than those of thermal efficiency must be taken into account before the suitability of a material to serve as a heat sink is decided. For instance, graphite has a low strength and it oxydizes easily at high temperatures while beryllium has poor ductility.

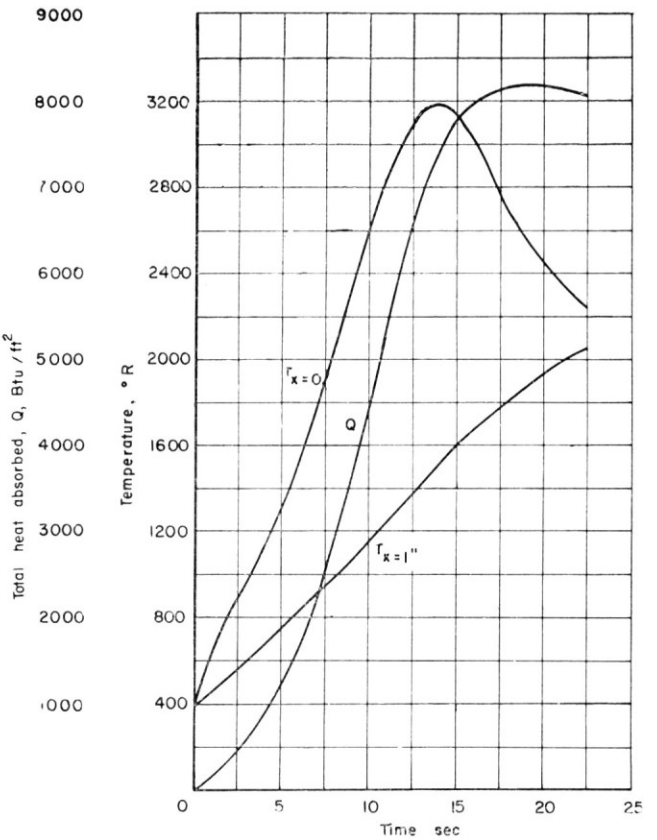

FIG. 12. Temperature history of graphite wall.
(from Ref. 20)

According to Refs. 21 and 22, however, the ductility of beryllium suffices for industrial use, particularly when the operating temperature is in the range from 500°F to 1500°F. The mechanical properties are excellent; at 1200°F the modulus of elasticity is 26×10^6 psi and the ultimate tensile strength about 21,000 psi. Thermal stresses in beryllium structural elements are often less dangerous than in other materials. This is due mostly to the low coefficient of thermal expansion of the material. Measured values are $6{\cdot}4 \times 10^{-6}$ per °F at 70°F and $12{\cdot}4 \times 10^{-6}$ per °F at 1200°F. The product of the expansion coefficient and Young's modulus is 282 lb in.$^{-2}$ °F^{-1} at 70°F and 322 lb in.$^{-2}$ °F^{-1} at 1200°F.

C. Melting

When the heating rate is so high that heat conduction cannot prevent the surface of the structure from reaching the melting temperature, the heat sink approach to the design of a re-entry vehicle becomes impossible.

There is no fundamental reason, however, why the designer should not permit the surface to melt if this process takes place slowly enough and in an orderly manner. The material of the vehicle, is of course, used up in this process but it is utilized more fully than in the heat sink. The maximum heat absorbed by the material is $c(T_m - T_0)$ per unit mass in the heat sink as compared to $c(T_m - T_0) + L$, where L is the latent heat of fusion, which is the minimum heat absorbed when melting is permitted.

For instance, in the case of beryllium the latent heat of melting is about 500 BTU/lb. If the data of Table I are used and the initial temperature is taken as 400°R, the heat absorption before melting is 1590 BTU/lb; as melting absorbs 500 BTU/lb, the gain is 31·5%. Moreover the molten metal is still capable of absorbing heat before it is carried away by the air flow. The latent heat of melting copper is 91 BTU/lb. Under the conditions mentioned its heat absorption before melting is 215 BTU/lb; hence the gain is 42%. As was stated earlier, graphite does not melt but sublimes. Its latent heat of sublimation is 10,800 BTU/lb. Its heat absorption before sublimation being 3330 BTU/lb, the gain is 324%.

The exact calculation of the melting process, of the removal of the molten material by the air flow, and of the details of the heat transfer through the boundary layer of air, the liquid and the solid is a complex problem. However, an appraisal of the order of magnitude of the quantities involved can be had without much difficulty. For this purpose one may assume that the heating rate H is constant; that the wall of the structural element is so thick that the conditions at the inside surface do not influence the process; that the molten metal is instantaneously and fully removed by the air flow; and that a steady-state solution of the problem exists in the sense that, after a transient phase, the rate of melting and the temperature distribution through the wall remain constant (if the distance is measured in a moving system of coordinates from the instantaneous location of the heated surface).

Under these conditions the heat H flowing through the wall per unit area per unit time must be equal to the heat transferred to the material that is removed during the same time. The weight of this material is $V\rho$ per unit area and unit time if ρ is the density and V the velocity of ablation. This material is brought from the initial temperature T_0 to the melting temperature T_m; in addition, it absorbs the latent heat of fusion L. The principle of the conservation of energy requires that

$$H = V\rho[c(T_m - T_0) + L] \tag{104}$$

from which the ablation rate is

$$V = (H/\rho)/[c(T_m - T_0) + L] \tag{105}$$

Here c is the specific heat of the material.

Assumption of a heating rate $H = 1000$ BTU ft^2 sec and use of the values given earlier result in ablation rates of 4·2, 2·97, and 0·364 in/min for copper, beryllium, and graphite, respectively.

This solution disregards the transient aspects of the melting problem. They were properly considered by Landau[23] who set up the problem in the following mathematical form:

$$c\rho(\partial T/\partial t) = (\partial/\partial x)[K(\partial T/\partial x)] \qquad s(t) < x < b \qquad t > 0 \qquad (106a)$$

$$T(x, 0) = T_0(x) \leqslant T_m \qquad 0 \leqslant \times \leqslant b \qquad t = 0 \qquad (106b)$$

$$(\partial T/\partial x) = 0 \qquad x = b \qquad t > 0 \qquad (106c)$$

$$H(t) = -K(\partial T/\partial x) + \rho L(\partial s/\mathrm{d}t) \qquad x = s(t) \qquad t > 0 \qquad (106d)$$

In these equations, t is time, K the thermal conductivity, L the latent heat of melting, s the location of the free heated surface, and b the thickness of the wall.

When these equations are applied to the semi-infinite wall ($b = \infty$) under steady-state conditions, equation (105) results as the solution. More generally, the solution in the case of the semi-infinite wall depends on the parameter

$$m = (\sqrt{\pi}/2)(c/L)(T_m - T_0) \qquad (107)$$

Closed-form solutions were presented for the limiting cases of $m = 0$ and $m = \infty$, and for other values of m the differential equation was integrated with the aid of relay calculators. Some of the results obtained are shown in Fig. 13.

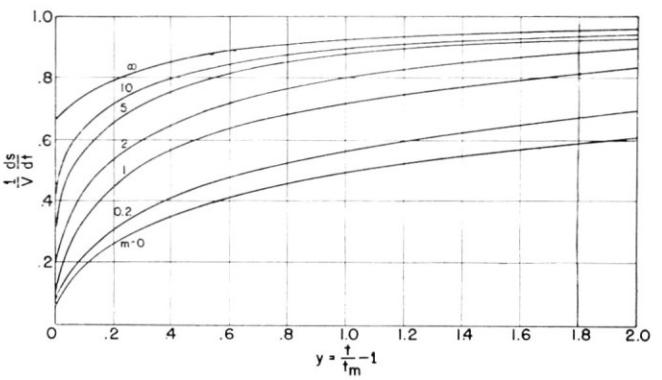

FIG. 13. Rate of melting ds/dt as fraction of the steady-state rate V (from Ref. 23)

The ordinate of the diagram is the ratio of the melting rate obtained to the steady-state melting rate V as given in equation (105). The abscissa is a nondimensional time quantity $(t/t_m) - 1$, where t_m is the melting

time, that is the time necessary for the wall $x = 0$ to reach the melting temperature:

$$t_m = (\pi/4)(Kc\rho/H^2)(T_m - T_0)^2 = [\rho(L/H)m]^2 a \tag{108}$$

Here a is the thermal diffusivity of the material:

$$a = K/c\rho \tag{109}$$

The figure shows that the velocity of ablation monotonically increases with time and asymptotically approaches the value V. At a time equal to twice the melting time, the velocity of ablation is about $0{\cdot}9V$ if m is greater than 5.

In a recent paper[24], Sutton developed a theory in which the assumption that the molten material vanishes instantaneously is not made. On the contrary, the flow of the melt is calculated from the laws of fluid dynamics. Since the Reynolds number based on a typical dimension is large, the equations are those of the incompressible boundary layer. For a two-dimensional flow they are given by Sutton as:

Continuity:

$$(\partial u/\partial x) + (\partial v/\partial y) = 0 \tag{110a}$$

Momentum:

$$\rho u(\partial u/\partial x) + \rho v(\partial u/\partial y) = -(\partial p/\partial x) + (\partial/\partial y)[\mu(\partial u/\partial y)] \tag{110b}$$

$$(\partial p/\partial y) = 0 \tag{110c}$$

Energy:

$$\rho C[u(\partial T/\partial x) + v(\partial T/\partial y)] = u(\partial p/\partial x) + (\partial/\partial y)[K(\partial T/\partial y)] + \mu(\partial u/\partial y)^2 \tag{110d}$$

The origin of coordinates is at the (moving) interface between the air flow and the molten material, x and y denote the directions parallel and perpendicular to the surface, u and v are the velocities of the fluid in the x and y directions, c is the specific heat at constant pressure, and p is the pressure. The boundary conditions at the interface ($y = 0$) are given in the form

$$V(0) = -m_i/\rho \qquad [\partial u(0)/\partial y] = \tau_i/\mu_i \qquad T(0) = T_i \tag{111}$$

Here T_i is the temperature of air and melt at the interface, m_i the mass transfer rate of the molten material across the interface in consequence of evaporation or burning and τ_i the shear stress between the molten material and the air. If the material exhibits a definite melting point, at a distance $y = y_\delta$ the conditions are:

$$T(\delta) = T_m \qquad u(\delta) = 0 \tag{112}$$

If this is not the case, the boundary conditions of equations (19) are replaced by

$$\lim_{y\to\infty} u(y) = 0 \qquad \lim_{y\to\infty} T(y) = T_0 \tag{113}$$

A suitable transformation reduced the partial differential equations to ordinary ones, which in turn were integrated with the aid of a REAC differential analyzer. In the numerical work average values were assumed for density, specific heat, and conductivity, but the variation of the viscosity with the temperature was duly taken into account. The material was taken as Pyrex glass and the density of the air over the surface was assumed as that prevailing at the stagnation point of a blunt body at a Mach number of 18 at an altitude of 90,000 ft.

Six interface temperatures ranging between 3000°F and 4000°F were considered as well as three values of the shear stress and two values of V at the interface (this defines m_i). It was found that τ_i and m_i had little effect on the interface temperature and the melting rate. These two quantities, however, increased approximately linearly with the rate of heat transfer through the interface. It was also observed that the temperature at the surface characterized by $u \simeq 0$ (boundary between liquid and solid) was about 62% of the interface temperature, and that the heat flow into the solid region was about 70% of the heat flow through the interface, if by this term the boundary between the air and the molten material is understood as before. The thickness of the molten glass for the flight condition mentioned earlier was calculated as 0·071 in. and the maximum tangential velocity u of the melt as 0·02% of the tangential velocity of the air stream outside the boundary layer.

D. Burning

When the heating rate becomes very high, the surface of the structure is likely to burn. The chemical reaction between the molecular or atomic oxygen and the atoms or molecules of the material of the structure is, however, not the only one to occur in the process. The various chemical species are transported from the surface of the structure into the boundary layer where they can undergo further changes through dissociation and recombination. For this reason the study of the effect of burning on the flow in the boundary layer and on the heat transfer from the boundary layer to the wall is far too complex to be treated here; an excellent summary of our present knowledge of the processes involved was recently given by Lees[25] at an AGARD panel meeting in Palermo.

In spite of the complexity of the problem, the case of laminar boundary layer flow has already been treated extensively. The equations governing the process become comparatively simple when the rate of heat energy transferred through diffusion is equal to that transferred through conduction. When this is true, the Lewis–Semenov number Le is equal to unity:

$$Le = \rho D_{12} \bar{c}_p / K = 1 \tag{114}$$

and the differential equation governing the rate of energy transport across streamlines has the same form as the ordinary heat conduction

equation for a non-reacting pure gas. In equation (114) $\bar{c}_p$ is the average specific heat at constant pressure of the gas mixture and D_{12} is the coefficient of mass diffusion of species 1 into species 2. To take care of more complex problems, approximate correction factors have been derived for cases when the value of *Le* differs from unity.

The conditions prevailing in a turbulent boundary layer are still largely unexplored. Fortunately a number of relatively simple formulas for the heat-transfer coefficient, derived on the basis of Reynolds' hypothesis of similarity between the turbulent transport of mass, momentum and energy, agree satisfactorily with experimental results.

Of considerable importance to the designer is the observation that burning is not necessarily fatal, or even disadvantageous, to the structure. When the heat of sublimation of the surface material is comparable to the heat released by combustion, the thickening of the boundary layer as well as other processes such as the dissociation of the sublimating material, may actually reduce the heat transfer to the structure below that observed without burning.

Acknowledgement—The author acknowledges his indebtedness to a number of his friends and co-workers for their advice and for help received in checking the text and in carrying out computations. These persons are Professors Daniel Bershader and Chi Chang Chao as well as Mr. Richard S. Lee and Mr. Edward J. Morgan.

REFERENCES

1. E. N. DA. C. ANDRADE, On the Viscous Flow of Metals, and Allied Phenomena, *Proc. Roy. Soc.* London (A), Vol. 84, No. A567, p. 1, June 1910.
2. N. J. HOFF, The Necking and the Rupture of Rods Subjected to Constant Tensile Loads, *J. Appl. Mech.*, Vol. 20, No. 1, p. 105, March 1953.
3. N. J. HOFF, Stress Distribution in the Presence of Creep, Chapter 12 of *High Temperature Effects in Aircraft Structures*, edited by N. J. Hoff, Pergamon Press, p. 248, London, 1958.
4. O. D. SHERBY and J. E. DORN, The Effects of Cold Rolling on the Creep Properties of Several Aluminum Alloys, *Trans. Amer. Soc. Metals*, Vol. 43, p. 622, 1950.
5. ANONYMOUS, Strength of Metal Aircraft Elements, ANC–5, U.S. Government Printing Office, Washington, D.C., March 1955.
6. FOREST C. MONKMAN and NICHOLAS J. GRANT, An Empirical Relationship Between Rupture Life and Minimum Creep Rate in Creep Rupture Tests, *Proc. Amer. Soc. Testing Materials*, Vol. 56, p. 593, 1956.
7. ELBRIDGE A. STOWELL, A Phenomenological Relationship Between Stress, Strain Rate, and Temperature for Metals at Elevated Temperatures, NACA–TN–4000, May 1957.
8. GEORGE J. HEIMERL and ARTHUR J. MCEVILY, JR., Generalized Master Curves for Creep and Rupture, NACA–TN–4112, October 1957.
9. T. J. I'A. BROMWICH, *An Introduction to the Theory of Infinite Series*, p. 334, MacMillan and Co., London, England, 1949.
10. EUGENE JAHNKE and FRITZ EMDE, *Tables of Functions*, Dover Publications, New York, N.Y., 1943.

11. N. J. Hoff, A Survey of the Theories of Creep Buckling, SUDAER No. 80, Stanford University Division of Aeronautical Engineering, Stanford, California, June 1958; also, Proceedings of the 3rd U.S. National Congress of Applied Mechanics, American Society of Mechanical Engineers, p. 29, New York, 1958.
12. B. Fraeijs de Veubeke, Creep Buckling, Chapter 13 of *High Temperature Effects in Aircraft Structures*, edited by N. J. Hoff, published for AGARD by Pergamon Press, p. 267, London, 1958.
13. Th. von Kármán, Untersuchungen über Knickfestigkeit, Mitteilungen über Forschungsarbeiten auf dem Gebiete des Ingenieurs-wesens, Verein Deutscher Ingenieure, Heft 81, Berlin, Germany, 1910.
14. N. J. Hoff, Effets thermiques dans le calcul de la résistance des structures d'avions et d'engins, Advisory Group for Aeronautical Research and Development (AGARD) of the North Atlantic Treaty Organization (NATO), Paris, January 1956.
15. Walter Ramberg and William R. Osgood, Description of Stress-Strain Curves by Three Parameters, NACA–TN–902, Washington, D.C., July 1943.
16. N. J. Hoff, Creep Buckling, *Aero. Qu.* Vol. 7, No. 1, p. 1, February 1956.
17. J. C. Chapman, Burton Erickson and N. J. Hoff, A Theoretical and Experimental Investigation of Creep Buckling, PIBAL Report No. 406, Polytechnic Institute of Brooklyn, Brooklyn, N.Y., October 1957.
18. N. J. Hoff, The Idealized Column, Grammel Anniversary Volume of Ingénieur-Archiv., Vol. 28, p. 89, 1959.
19. H. S. Carslaw and J. C. Jaeger, *Conduction of Heat in Solids*, Clarendon Press, Oxford, 1947.
20. Jackson R. Stalder, The Useful Heat Capacity of Several Materials for Ballistic Nose Cone Construction, NACA–TN–4141, November 1957.
21. L. A. Riedinger and R. E. Foster, Beryllium Applications in Structural Design, Lockheed Missile Systems Division Report LMSD 2643, Sunnyvale, California, January 1958.
22. J. A. Johnson, Re-entry Bodies and Beryllium, Lecture delivered at the Metals and Missiles Technical Session of the Space Age Conference sponsored by the Los Angeles Chamber of Commerce in Los Angeles on March 21, 1958.
23. H. G. Landau, Heat Conduction in a Melting Solid, *Qu. Appl. Math.*, Vol. 8, No. 1, p. 81, April 1950.
24. George W. Sutton, The Hydrodynamics and Heat Conduction of a Melting Surface, *J. Aero. Sci.*, Vol. 25, No. 1, p. 29, January 1958.
25. Lester Lees, Convective Heat Transfer with Mass Addition and Chemical Reactions, lecture presented at the Third Combustion and Propulsion Colloquium of the Advisory Group for Aeronautical Research and Development (AGARD) of the North Atlantic Treaty Organization (NATO) in Palermo, Italy, March 17–21, 1958; to be published by AGARD.

DISCUSSION

H. P. van Leeuwen*: This comment, which is a written one, differs from the one given verbally because in the Discussion it did not become fully clear what the comment implied.

The essence is that it is questioned whether Prof. Hoff consistently used the concept of natural strain in his calculations given in pages 735–939.

* National Aeronautical Research Institute, Amsterdam, Holland.

It should be noted that he did, in fact, introduce this concept in equation (10) on p. 5, which may be read as

$$\frac{\mathrm{d}}{\mathrm{d}t}\,[\log(1+\epsilon)] = \epsilon_{\mathrm{n}} = f(\sigma) \tag{10}$$

He, however, abandons it on p. 6 when he writes:

$$t_{\mathrm{cr}} \simeq \int^{\infty} \frac{\mathrm{d}\log\sigma}{f(\sigma)} = \int^{\infty} \frac{\mathrm{d}\log\sigma}{\dot{\epsilon}}$$

and thus assumes $f(\sigma) = \dot{\epsilon}$ which if course is not in accordance with equation (10) as given previously.

N. J. HOFF: The author is willing to admit that the second part of equation (18) may be misleading; it would have been preferable to write $\dot{\epsilon}_{\mathrm{n}}$ instead of $\dot{\epsilon}$. On the other hand, this equation was used only in the graphical construction in connection with creep rate data presented in graphs. As the steady creep rates plotted in these graphs were obtained largely from test points corresponding to strains not exceeding a few per cent, the distinction between engineering strain and natural strain is unnecessary. Hence the graphic integration indicated in Fig. 1 is permissible.

In the analytical work the critical time was calculated from equations (15) and (27) and from the first part of equation (18) in which the distinction between natural strain and engineering strain is not subject to any doubt.